Ab initio study of phosphorus anodes for lithium and sodium-ion batteries

Martin Mayo,[†] Kent J. Griffith,[‡] Chris J. Pickard,[¶] and Andrew J. Morris[*,†]

Theory of Condensed Matter Group, Cavendish Laboratory, University of Cambridge, J. J. Thomson Avenue, Cambridge CB3 0HE, United Kingdom, Department of Chemistry, University of Cambridge, Lensfield Road, Cambridge CB2 1EW, United Kingdom, and Department of Materials Science and Metallurgy, 27 Charles Babbage Rd, Cambridge CB3 0FS, United Kingdom

E-mail: ajm255@cam.ac.uk

Abstract

Phosphorus has received recent attention in the context of high-capacity and high-rate anodes for lithium and sodium-ion batteries. Here, we present a first principles structure prediction study combined with NMR calculations which gives us insights into its lithiation/sodiation process. We report a variety of new phases found by the *ab initio* random structure searching (AIRSS) and the atomic species swapping methods. Of particular interest, a stable Na_5P_4–C2/m structure and locally stable structures found less than 10 meV/f.u. from the convex hull, such as Li_4P_3–$P2_12_12_1$, NaP_5–Pnma and Na_4P_3–Cmcm. The mechanical stability of Na_5P_4–C2/m and Li_4P_3–$P2_12_12_1$ has been studied by first principles phonon calculations. We have calculated average voltages which suggests that black phosphorus (BP) can be considered as a

[*]To whom correspondence should be addressed
[†]University of Cambridge
[‡]University of Cambridge
[¶]University of Cambridge

safe anode in lithium-ion batteries due to its high lithium insertion voltage, 1.5 V; moreover, BP exhibits a relatively low theoretical volume expansion compared with other intercalation anodes, 216% ($\Delta V/V$). We identify that specific ranges in the calculated shielding can be associated with specific ionic arrangements, results which play an important role in the interpretation of NMR spectroscopy experiments. Since the lithium-phosphides are found to be insulating even at high lithium concentrations we show that Li-P-doped phases with aluminium have electronic states at the Fermi level suggesting that using aluminium as a dopant can improve the electrochemical performance of P anodes.

Introduction

Owing to their relatively high specific energy and capacity, Li-ion batteries (LIBs) are the energy source of choice for portable electronic devices.[1] Despite the vast technological advances made since the first commercial LIB was released by Sony in 1991, the specific energy of commercial LIBs is limited to approximately 250 Whkg^{-1}, which is half the estimated need for a family car to travel 300 miles without recharge.[2] The demand of higher specific energies and capacities motivates the study of novel materials for the next generation of LIBs. In almost all conventional LIBs available for commercial use the cathode is typically a transition layered metal oxide, $LiMO_2$, with M=Co, Ni, Mn, etc, and the anode material is graphite.[2–4] Intercalation electrodes experience slight changes during charge and discharge, *e.g.*, less than 7% volume change in C negative electrodes,[3] leading to a high capability of retaining their capacity over charge/discharge cycles. However, these electrodes suffer from low specific capacity due to the limited intercalation sites available for Li ions in the host lattice,[5] *e.g.*, 372 mAhg^{-1} for graphite. In order to overcome the capacity limitation of intercalation anodes, it has been suggested to use different alloys of lithium as LIB anodes.[3,5–9] A wide range of materials have been studied for this purpose, such as group IV and V elements, magnesium, aluminium and gallium among others.[3,7] Alloy materials can achieve 2-10 times higher capacity compared to graphite anodes, where the highest capacity is achieved by silicon, 3579 mAhg^{-1}.[10] However, alloys tend to undergo relatively large structural changes under

lithiation,[2,3,7,10] leading to a poor cycle life.

Due to the high abundance, low cost, and relatively uniform geographical distribution of Na, Na-ion batteries (NIBs) have received recent attention. Despite some disadvantages, such as its larger ionic radius (1.02 Å compared to 0.76 Å for Li) and the lower cell potential of most Na systems,[11] NIBs are considered to be one of the most promising alternatives to meet large-scale electronic storage needs.[12] In spite of similarities between elemental Li and Na, Na systems present significantly different kinetic and thermodynamic properties.[9] The widely used graphite negative anode in LIBs is not successful for NIBs[13] due to a poor specific capacity and bad cyclability. The Si alloy suggested for LIBs is not suitable for NIBs as the Na concentration in Na-Si systems is limited to 50 %,[12] therefore most recent studies have focused on Na-Sn and Na-Sb systems.[12]

Reaction of phosphorus with three Li or Na atoms produces Li_3P[14] and Na_3P[15] respectively; which corresponds to a large theoretical capacity of 2596 $mAhg^{-1}$ and theoretical volume expansion $\Delta V/V$ of 216 % for Li_3P and 391 % for Na_3P from black phosphorus (BP). Of the several known allotropes, black phosphorus, red phosphorus, and the recently synthesised phosphorene[16] have been studied as candidates for LIB and NIB anodes.[17–19] Recent experimental studies[9,20–25] showed that the addition of carbon to the phosphorus anode leads to an improvement in the reversibility of charge/discharge processes, probably due to an enhancement in its electrical conductivity and mechanical stability. The study conducted by Qian *et al.*,[9,24] showed that amorphous phosphorus/carbon nano composite anodes are capable of achieving relatively high storage capacities per total mass of composite, 2355 $mAhg^{-1}$ for LIBs and 1765 $mAhg^{-1}$ for NIBs, good capacity retention after 100 cycles and high power capabilities at high charge/discharge rates. Recently, a phosphorus-graphene hybrid has been proposed as anode material for LIBs[26] and NIBs[27] showing improved electrochemical performances.

All the experimental studies agree that Li_3P and Na_3P are formed during the discharge process; however, the formation of other phases during the lithiation/sodiation process remains unclear. In the case of LIBs, differential capacity plots suggest the formation of Li_xP phases, however the assignment of the XRD spectra can be challenging.[9,19,20,24] In a study presented by Sun *et al.*[21] it

has been suggested, based on *ex situ* XRD, that crystal phases of Li-P form at the end of the charge. Recently,[28] an *ab initio* molecular dynamics (AIMD) study suggested an amorphous-to-crystalline phase transition in Li-P. AIMD has been also recently applied to Na-P,[29] where a change from an intercalation to an alloying sodiation process at $Na_{0.25}P$ has been proposed.

During Li/Na insertion and extraction, anodes are expected to form non-equilibrium structures. Evidence of a metastable structure formation in the Li-P system has been reported by Park *et al.*,[20] where the authors suggested the formation of Li_2P phase during the first discharge based on an electrochemical study. In the case of the well studied Li-Si system, the lithiation induces an electrochemical solid phase amorphisation, where the crystalline Si is consumed to form a Li_xSi amorphous phase;[5] nevertheless, the equilibrium crystalline compounds are generally used as a first step in order to study the electromechanical process (See Ref. 12 and references therein).

Ab initio techniques have been shown to be successful in giving insights into a better understanding of different processes occurring in an electrode.[30–32] From total energies, important properties of an electrode like voltage profiles and volume change can be estimated. In addition, NMR parameters can be calculated for certain systems offering a powerful method to understand the local structure of the studied system as well as a way of complementing experimental studies. First principles ^{31}P NMR calculations were successfully applied to study calcium phosphates[33] and aluminophosphates,[34] where good agreement between experimental and calculated NMR data was reported.

In this work, we present an *ab initio* study of Li-P and Na-P compounds. We first perform a structure prediction study combining atomic species swapping along with *ab initio* random structure searching methods for the Li-P and Na-P systems. We report various new stable and metastable structures and suggest connections between lithium/sodium contents and expected ionic arrangements. Lithiation/sodiation processes are assessed by calculating average voltage profiles, electronic density of states and NMR chemical shielding of the ground state phases, allowing us to predict the local environment evolution of P under lithiation/sodiation. We conclude showing the effect of dopants on the electronic structure of Li-P compounds, where we propose doping the

anode with aluminium in order to improve the anode performance.

Methods

Structure prediction was performed using the *ab initio* random structure searching method (AIRSS).[35] For a given system, AIRSS initially generates random structures which are then relaxed to a local minima in the potential energy surface (PES) using DFT forces. By generating large numbers of relaxed structures it is possible to widely cover the PES of the system. Based on general physical principles and system-specific constraints, the search can be biased in a variety of sensible ways.[36] About 20000 Li-P structures and 5000 Na-P structures were generated by AIRSS. The fewer structures for the Na-P system were due to the accuracy of the Na pseudopotential required for the searches and the larger basis set, which made the search considerably more expensive computationally. The phase space explored by the AIRSS method was extended by relaxing experimentally obtained crystal structures. All combinations of {Li,Na,K}-{N,P,As,Sb} crystal structures at different stoichiometries were obtained from the International Crystallographic Structure Database (ICSD). For each structure, the anions and cations were swapped to Li/Na and P respectively and then relaxed using DFT forces. The AIRSS + species swapping method has been successfully used for Li-Si,[37] Li-Ge[32,37] and Li-S[31] systems. Furthermore, a study on point defects in silicon has been presented[38,39] using the AIRSS method.

AIRSS calculations were undertaken using the CASTEP DFT plane-wave code.[40] The gradient corrected Perdew Burke Ernzerhof (PBE) exchange-correlation functional[41] was used in all the calculations presented in this work. The core electrons were described using Vanderbilt "ultrasoft" pseudopotentials, the Brillouin zone was sampled using a Monkhorst-Pack grid[42] with a k-point spacing finer than $2\pi \times 0.05$ Å^{-1}. The plane wave basis set was truncated at an energy cutoff value of 400 eV for Li-P and 500 eV for Na-P.

The thermodynamical phase stability of a system was assessed by comparing the free energy of different phases. From the available DFT total energy of a given binary phase of elements A

and B, $E\{A_aB_b\}$, it is possible to define a formation energy per atom,

$$E_f/\text{atom} = \frac{E\{A_aB_b\} - aE\{A\} - bE\{B\}}{a+b}. \quad (1)$$

The formation energies of each structure were then plotted as function of the B element concentration, $u = \frac{b}{a+b}$, starting at $u = 0$ and ending at $u = 1$. A convex hull was constructed between the chemical potentials at $(u, E_f/\text{atom}) = (0,0);(1,0)$ drawing a tie-line that joins the lowest energy structures, provided that it forms a convex function. This construction gives access to the 0 K stable structure as the second law of thermodynamics demands that the (free) energy per atom is a convex function of the relative concentrations of the atoms (see Figure 1).

Average voltages for the structures lying on the hull were calculated from the available DFT total energies. For two given phases on the hull, $A_{x_1}B$ and $A_{x_2}B$ with $x_2 > x_1$, the following two phase reaction is assumed,

$$A_{x_1}B + (x_2 - x_1)A \rightarrow A_{x_2}B. \quad (2)$$

The voltage, V, is given by,[43]

$$\begin{aligned} V &= -\frac{\Delta G}{x_2 - x_1} \approx -\frac{\Delta E}{x_2 - x_1} \\ &= -\frac{E(A_{x_2}B) - E(A_{x_1}B)}{x_2 - x_1} + E(A), \end{aligned}$$

where it is assumed that the Gibbs energy can be approximated by the internal energy, as the pV and thermal energy contributions are small.[43]

The low energy structures obtained by the AIRSS search were refined with higher accuracy using a k-points spacing finer than $2\pi \times 0.03\text{Å}^{-1}$ and an energy cut-off of 650 eV for Li-P and 800 eV for Na-P and more accurate pseudopotentials [1]. The structures obtained from the ICSD were relaxed with the same level of theory and the formation energies and voltages were obtained. The

[1] Pseudopotentials generated by the CASTEP on-the-fly generator:
Li 1|1.2|10|15|20|10U:20(qc=6)
Na 2|1.3|1.3|1.0|16|19|21|20U:30U:21(qc=8)
P 3|1.8|2|4|6|30:31:32

same level of accuracy was used to calculate the nuclear magnetic shielding of the structures on the convex hull employing the gauge-including-projector-augmented-wave (GIPAW) algorithm[44] implemented in CASTEP and the electronic density of states. The latter were calculated with the OptaDOS code[45] using the linear extrapolative scheme.[46,47] Phonon dispersion curves were calculated using Density Functional Perturbation Theory in CASTEP.[48] Norm-conserving pseudopotentials [2] were used, the Brillouin zone was sampled using a Monkhorst-Pack grid[42] with a k-point spacing finer than $2\pi \times 0.03$ Å^{-1} and the plane wave basis set was truncated at an energy cut-off of 1000 eV. The structures were fully relaxed at this level of accuracy. The NMR parameters and density of states of black P were calculated with the CASTEP semi empirical dispersion correction (SEDC).[49] The scheme of Grimme (G06)[50] was used following a successful previous application to black P.[51] SEDCs were not used for all compounds in the convex hull, as their effect on the energetics of bulk metals and layered phases remains unclear.[52,53]

Results

Lithium phosphide

Figure 1 shows the formation energy as a function of lithium concentration of the low-energy structures obtained by the search. The stable structures found on the convex hull, in increasing lithium concentration order, are black P–Cmca, LiP_7–$I4_1/acd$,[54] Li_3P_7–$P2_12_12_1$,[55] LiP–$P2_1/c$,[56] Li_3P–$P6_3/mmc$[57] and Li–$Im\bar{3}m$. A novel DFT Li_4P_3–$P2_12_12_1$ phase is found 4 meV/f.u. above the convex hull, well within DFT accuracy. All the known Li-P phases are found on the convex hull, except for LiP_5–$Pna2_1$[54] which is found 12 meV/f.u. from the convex tie-line in our 0 K DFT calculation. The average voltage profile was calculated between pairs of proximate stable structures relative to Li metal. A plot of the average voltages as a function of Li concentration is

[2]Pseudopotentials generated by the CASTEP on-the-fly generator:
Li 1|1.2|18|21|24|10N:20N(qc=8)
Na 2|1.5|20|23|26|20N:30N:21N(qc=8)
P 1|1.6|6|7|8|30N:31L:32N

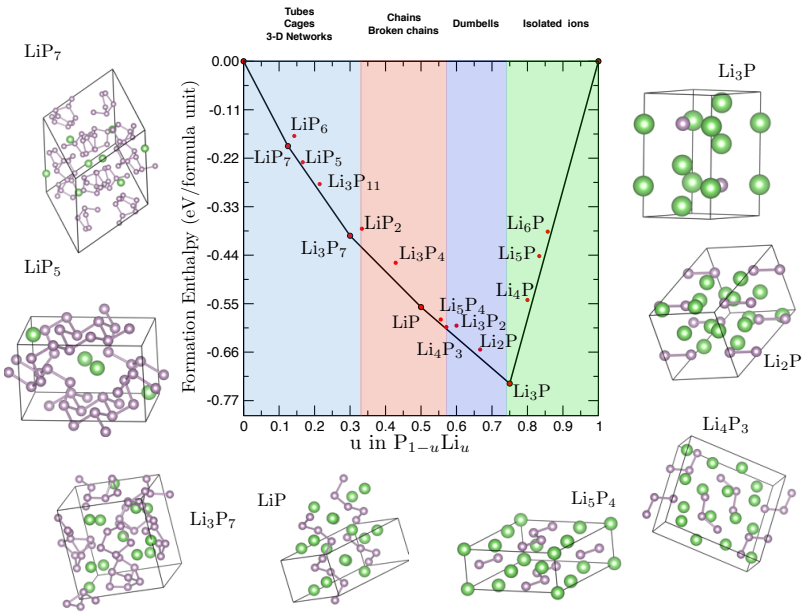

Figure 1: Formation enthalpy per atom versus the fractional lithium concentration in the Li-P compound. The convex hull (tie-line) is constructed by joining the stable structures obtained by the searches. The convex hull has been divided in four main regions to guide the eye, highlighting the kind of ionic arrangement in each region. Selected structures are shown with green and purple spheres denoting Li and P atoms, respectively, with the purple lines indicating P–P bonds. For a full description of the phases, see Table 1.

presented in Figure 2.

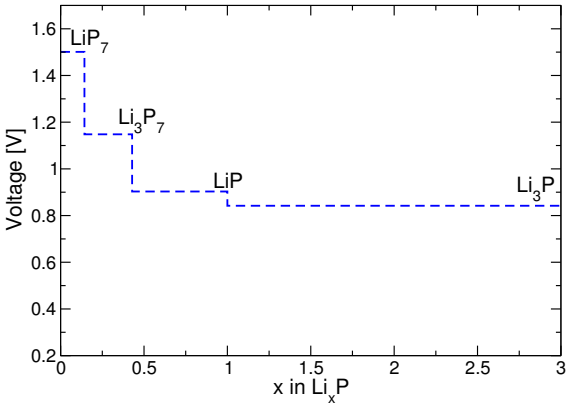

Figure 2: Average voltages relative to lithium metal calculated for the structures found on the convex hull (Figure 1).

Table 1 summarises the structures presented in Figure 1. The convex hull construction reveals new metastable structures, which are of importance when studying the lithiation process of the anode during cycling, as the anode is unlikely to reach thermodynamic equilibrium during charge and discharge. We identify that the structures can be categorised in four main regions according to their P ionic arrangement, as is highlighted in Figure 1. As the Li concentration is increased, the structures change as following: tubes, cages and 3-D networks $\rightarrow$ chains and broken chains $\rightarrow$ P dumbbells $\rightarrow$ isolated P ions.

For $0 \leq x \leq 0.5$ in Li_xP structures are composed mainly by tubes, cages and 3-D networks where threefold P bonding is mainly favoured. The least lithiated phase found on the hull is LiP_7 which shows tubular helices of connected P_7 cages along the [001] axis. LiP_6–$R\bar{3}m$ and LiP_5–$Pna2_1$ exhibit relatively similar structures formed by a 3-D networks with the majority of the P ions threefold bonded. The next structure found on the convex hull is Li_3P_7, where the phosphorus tubes are broken, forming isolated P_7 cages dispersed in the 3D structure. AIRSS has found a LiP_2–$P2_1/c$ structure 41 meV/f.u. above the convex hull. The structure is formed of 2-D layers of phosphorus arranged in a distorted armchair-like fashion.

In the $0.5 < x < 1.33$ region the structures are significantly different, tending to form chains and broken chains. The structure of Li_xP_x, x=5-9, has recently received attention in the context

Table 1: Description of the experimental and predicted Li_xP phases. We indicate with a star ($\star$) the stable phases which are found on the convex hull. We identify four main regions with different ionic arrangements: for $0 \leq x \leq 0.5$; the structures show tubes, cages and 3-D networks composed of three and two phosphorus bonds, for $0.5 < x < 1.33$; phosphorus chains and broken chains, for $1.33 < x \leq 2$; phosphorus dumbbells and for concentrations larger than $x = 2$ the structures are mainly composed of isolated phosphorus ions. The CIF files of the structures obtained by AIRSS and the swapping method can be found in the Supporting Information.

Stoichometry	x in Li_xP	Distance from the hull [eV/f.u.]	Space group	Structure origin	Description
black-P $\star$	0		Cmca		
LiP_7 $\star$	0.143		$I4_1/acd$	Known Li-P phase[54]	P tubes
LiP_6	0.167	0.046	$R\bar{3}m$	AIRSS	P 3-D network
LiP_5	0.2	0.012	$Pna2_1$	Known Li-P phase[54]	P 3-D network
Li_3P_{11}	0.273	0.017	Pbcn	Swapping from Na_3P_{11}[58]	P_{11} cages
Li_3P_7 $\star$	0.429		$P2_12_12_1$	Known Li-P phase[55]	P_7 cages
LiP_2	0.5	0.041	$P2_1$	AIRSS	Black P - like layers
Li_3P_4	0.75	0.043	C2/m	AIRSS	Chair-like chains
LiP $\star$	1		$P2_1/c$	Known Li-P phase[56]	P helix
Li_5P_4	1.3	0.012	C2/m	Swapping from Na_5As_4[59]	4 P zig-zag chains
Li_4P_3	1.333	0.006	$P2_12_12_1$	AIRSS	3 P zig-zag chains
Li_3P_2	1.5	0.03	Pm	AIRSS	P dumbbells
Li_2P	2	0.02	$P2_1/c$	AIRSS	P dumbbells
Li_3P $\star$	3		$P6_3/mmc$	Known Li-P phase[57]	Isolated P ions
Li_4P	4	0.044	C2/m	AIRSS	Isolated P ions
Li_5P	5	0.046	Cmma	AIRSS	Isolated P ions
Li_6P	6	0.033	$P\bar{1}$	AIRSS	Isolated P ions
Li $\star$			$Im\bar{3}m$		

of inorganic double-helix structures,[60] where it was shown that AIRSS predicts the $P2_1/c$ symmetric Li_1P_1 bulk phase; moreover, the stability of an isolated double-helix was demonstrated by phonon calculations. Two phases are found very close to the hull in this region, Li_5P_4 and Li_4P_3. Li_4P_3–$P2_12_12_1$ is an AIRSS structure with a formation enthalpy 4 meV/f.u. above the tie-line, a difference which is within DFT accuracy. Li_5P_4–C2/m was obtained by swapping ions from Na_5As_4[59] and it is found 10 meV/f.u. above the convex hull. Both structures are formed by three (Li_4P_3) and four-bonded (Li_5P_4) in-plane chains, see Figure 1 for an illustration. We have explored the possible mechanical stability of Li_4P_3–$P2_12_12_1$ by performing a phonon calculation, the calculated phonon dispersion is presented in Figure 3. The stability of a structure in terms of lattice

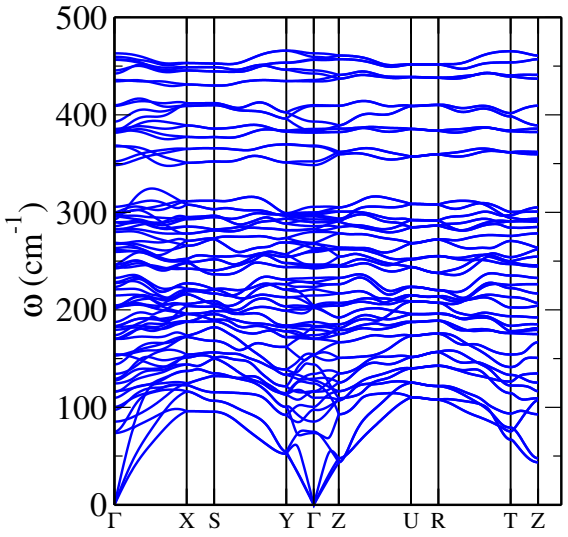

Figure 3: Phonon dispersion curve of Li_4P_3– $P2_12_12_1$. The absence of any imaginary frequency in the Brillouin zone confirms the stability of a structure in terms of lattice dynamics.

dynamics is confirmed by the absence of any imaginary frequency in the Brillouin zone. AIRSS predicts a Li_3P_4–C2/m structure 43 meV/f.u. above the convex hull, composed of chair-like chains of phosphorus ions.

For $1.33 < x \leq 2$ two structures are found by AIRSS, Li_2P–$P2_1/c$ and Li_3P_4–C2/m, which form P-P dumbbells. Dumbbell formation in Li-X (X=S,Si,Ge) systems, has played an important role in the interpretation of the electrochemical behaviour in terms of structure transformation.[32,37]

For concentrations larger that x=2 the P structures are formed by isolated P ions. The most

lithiated phase found on the convex hull is Li_3P,[14] a phase which is generally observed at the end of discharge in electrochemical experiments.[9,20,24] Three more structures are found by the AIRSS searches for $x > 3$, Li_4P, Li_5P and Li_6P, all of them composed of isolated P atoms.

From the obtained geometry optimised lattice constants, we calculate the volume change of P as it is lithiated. Phosphorus undergoes a relatively small volume expansion compared to other typical volume changes of *ca.* 300 % in other intermetallic Li. The resulting volume per P atoms and volume change are summarised in Table 2.

Table 2: Volume change calculated for the stable Li-P phases found on the convex hull relative to black phosphorus. Phosphorus undergoes a relatively small volume expansion compared to other typical volume changes of *ca.* 300 % in other intermetallic Li. The volume changes were calculated using the DFT–PBE lattice parameters.

x in Li_xP	Volume per P atom (Å^3)	Volume change (%)
0	19.28	
1/7	24.75	28.37
3/7	28.34	47
1	31.29	63.32
3	58.37	202.78

The electronic density of states (eDOS) of the structures found on the convex hull were calculated with the OptaDOS code[45] and are shown in Figure 4. All structures, except for Li, show a semiconducting-like eDOS, which is surprising especially for the phases with high lithium concentration.

The experimental ability of measuring NMR spectra during charge and discharge, can be an extremely powerful tool to elucidate the structural evolution of the anode during the lithiation.[30] We have calculated the phosphorus chemical shielding for the stable structures of the Li-P system. We have included the LiP_5 $Pna2_1$ chemical shielding calculation for comparison with the experimental data reported in Ref. 61. A plot of the correlation between the calculated and experimental NMR parameters of LiP_5,[61] Li_3P[23] and black P[25] is presented in Figure 5, where a good correlation is seen between experimental and calculated values.

The resulting NMR parameters of all the structures are illustrated in Figure 6. A general trend is observed in chemical shift, where the latter increases with the Li concentration in Li_xP. We

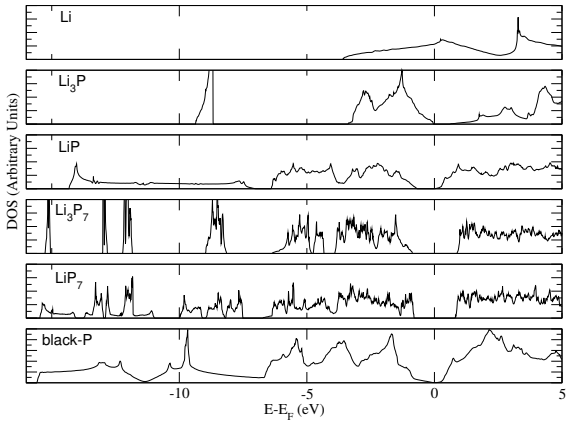

Figure 4: Total electronic density of states of the Li-P phases found on the convex hull. The Li-P structures exhibit a semiconductor-like eDOS even for high Li concentrations.

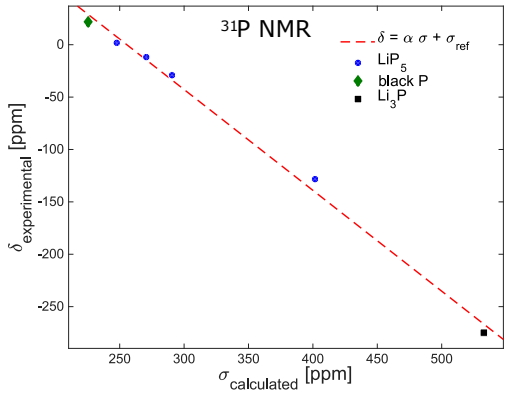

Figure 5: Correlation between the ^{31}P NMR calculated chemical shielding, $\sigma_{calc.}$, and experimental chemical shifts, $\delta_{exp.}$, referenced relative to an 85% H_3PO_4 aqueous solution for LiP_5[61] Li_3P[23] and black P.[25] The data was fitted to a linear function $\delta_{exp.} = \alpha\sigma_{calc.} + \sigma_{ref.}$ with resultant fitting parameters $\alpha = -0.96 \pm 0.1$ and $\sigma_{ref.} = 245.9 \pm 34.1$. The deviation of α from the ideal value of -1 is well known when correlating between calculated shielding and experimental shifts (See Ref.[62] for details), the obtained $\sigma_{ref.}$ was used to reference the presented NMR results (See Figures 6 and 11). Our resulting α and β are in agreement with Refs. 33,34 within the reported uncertainty.

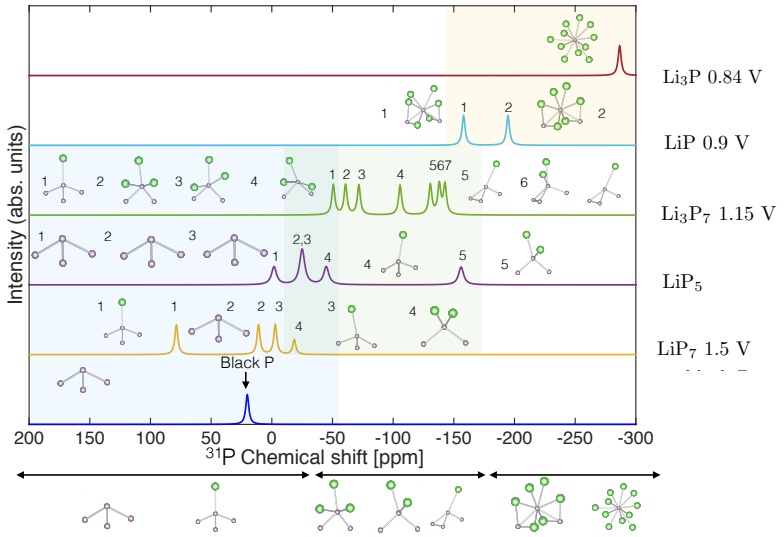

Figure 6: Calculated ^{31}P NMR chemical shifts, referenced using $\sigma_{ref.}$ obtained from Figure 5, for various Li-P compounds showing the change in chemical shift as the local environment of phosphorus changes. For visualisation purposes a Lorentzian broadening is assigned to the calculated ^{31}P NMR parameters. For each crystallographic site a cluster with a radius of 3 Å is shown and labeled accordingly. We have coloured the background to guide the eye between the three regions, above -45 ppm, below -155 ppm and an intermediate region. Above -45 ppm ppm predominantly the structures have three phosphorus nearest neighbours (NNs) and one or no lithium NN. Below -155 ppm the phosphorus has more than six lithium NNs. In the intermediate region the phosphorus ions tends to have four or five NNs of which two to three are phosphorus atoms.

identify three main regions in the chemical shift described in Figure 6 which can be roughly related to the amount of lithium and phosphorus nearest neighbours (See caption in Figure 6 for detailed description).

Sodium phosphide

Na-P forms similar structures to those found for Li-P, as expected due to their similar chemistry. However, the convex hull of the NaP system, as shown in Figure 7, exhibits two main differences: first, the Li_1P_1 phase has a lower formation energy than Na_1P_1 by approximately -0.125 eV, the second is that the Li_3P phase has lower formation energy than Li_1P_1 by -0.125 eV, whereas Na_3P has higher formation energy than Na_1P_1 by 0.05 eV/f.u.. These differences are manifested in the calculated average voltages (see Figures 8 and 2), where the Na-P voltage profile drops to lower values at high Na concentrations. The stable phases predicted by the DFT calculations are

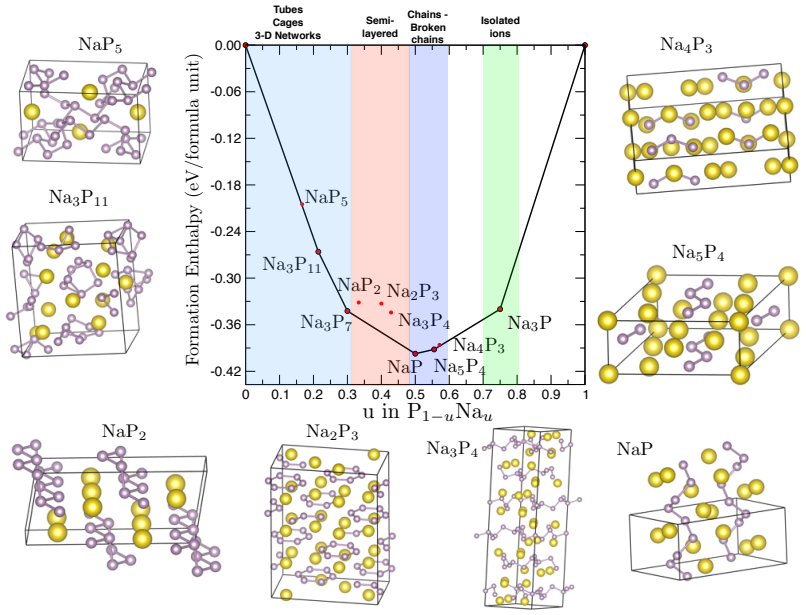

Figure 7: Formation enthalpy per atom vs the fractional sodium concentration in the Na-P compound. The convex hull (tie-line) is constructed by joining the stable structures obtained by the searches.

summarised in Table 3.

The least sodiated Na-P structure found in the Na-P convex hull construction is a locally stable

Table 3: Description of the experimental and predicted Na_xP phases. We indicate with a star ($\star$) the stable phases which are found on the convex hull. The Na-P structures show similar ion arrangements as those observed in Li-P (see Figure 1 for illustration), with differences in the $0.45 < x < 1$ region and the absence of phosphorus dumbbells. The CIF file of the structure obtained by AIRSS and swapping method can be found in the Supporting Information.

Stoichometry	x in Na_xP	Distance from the hull [eV/f.u.]	Space group	Structure origin	Description
black-P $\star$	0		Cmca		
NaP_5	0.2	0.002	Pnma	Swapping from LiP_5 [54]	P 3-D network
Na_3P_{11} $\star$	0.273		Pbcn	Known Na-P phase [58]	P_{11} cages
Na_3P_7 $\star$	0.429		$P2_12_12_1$	Known Na-P phase [55]	P_7 cages
NaP_2	0.5	0.02	C2/m	Swapping from KSb_2 [63]	Black P - like broken layers
Na_2P_3	0.667	0.037	Fddd	Swapping from K_4P_6 [64]	P six-fold rings
Na_3P_4	0.75	0.034	$R\bar{3}c$	AIRSS	In-plane connected chains
NaP $\star$	1		$P2_1/c$	Known Na-P phase [56]	P helix
Na_5P_4 $\star$	1.25		C2/m	Swapping from Na_5As_4 [59]	4 P zig-zag chains
Na_4P_3	1.333	0.002	Cmcm	Swapping from K_4P_3 [65]	4 P zig-zag chains
Na_3P $\star$	3		$P6_3cm$	Swapping from Na_3As [59]	Isolated P ions
Na_3P	3	0.005	$P6_3/mmc$	Known Na-P [14]	Isolated P ions
Na $\star$			$Im\bar{3}m$		

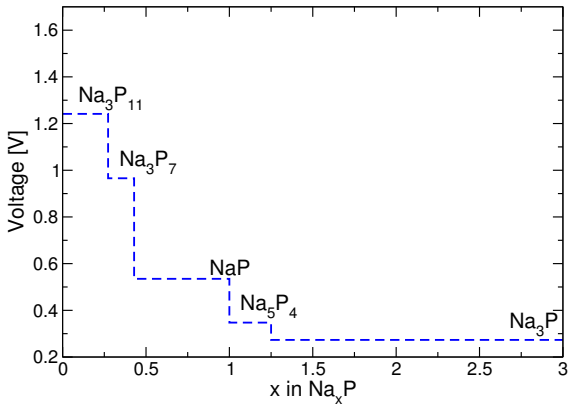

Figure 8: Average voltages relative to sodium calculated for the structures found on the convex hull (Figure 7).

NaP_5– Pnma phase, which was obtained by swapping species from LiP_5.[54] Increasing in sodium content, two known phases are found on the convex hull, Na_3P_{11}–Pbcn[58] and Na_3P_7–$P2_12_12_1$.[55] In the $0.45 < x < 1$ region we find three structures with rather different ionic arrangements, exhibiting broken black P - like layers (NaP_2– C2/m[63]), P six-fold rings (Na_2P_3–Fddd[64]) and in-plane connected chains (Na_3P_4–$R\bar{3}c$ predicted by AIRSS). For $x > 1$ the structures show similar arrangements as in the Li-P system, although, unlike in Li-P, Na-P does not seem to favour dumbbell formations. The Na_5P_4–C2/m obtained by swapping atoms from Na_5As_4[59] exhibits a layered structure consisting of Na sheets separated by four-bounded in-plane P chains. This new phase is predicted to be thermodynamically stable by our calculations. Furthermore, its calculated phonon dispersion presented in Figure 9 curve confirms the stability of the phase in terms of lattice dynamics. The volume changes were calculated as for Li-P and are shown inTable 4.

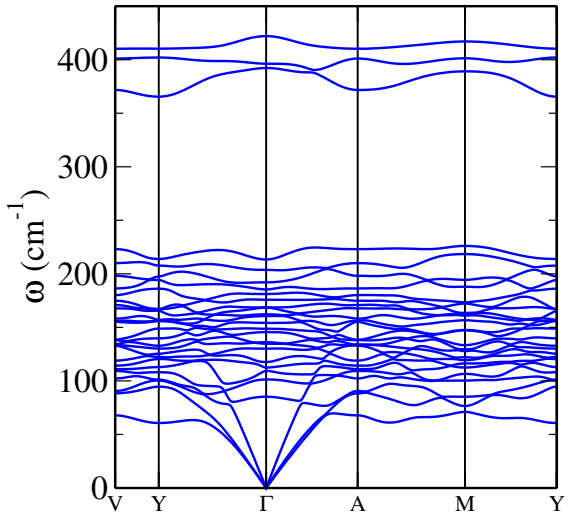

Figure 9: Phonon dispersion curve of Na_5P_4–C2/m. The absence of any imaginary frequency in the Brillouin zone confirms the stability of a structure in terms of lattice dynamics.

As in the Li-P system, the Na-P phases exhibit a semiconducting behaviour, except for the Na_5P_4 phase which shows a finite value of eDOS at the Fermi energy.

Table 4: Volume change calculated for the stable Na-P phases found on the convex hull relative to black phosphorus. The volume changes were calculated using the DFT–PBE lattice parameters.

x in Na_xP	Volume per P atom ($Å^3$)	Volume change (%)
0	19.28	
3/11	29.98	55.50
3/7	36.25	88.04
1	42.33	119.58
5/4	49.37	156.10
3	94.89	392.25

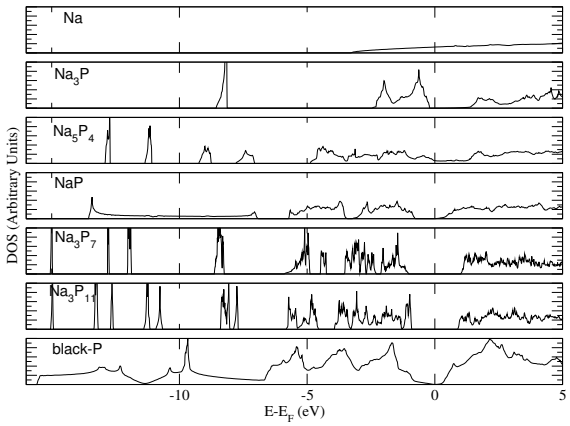

Figure 10: Total electronic density of states of the Na-P phases found on the convex hull. The Na-P phases exhibit a semiconductor-like eDOS, except for the Na_5P_4 which has a finite value of eDOS at the Fermi level.

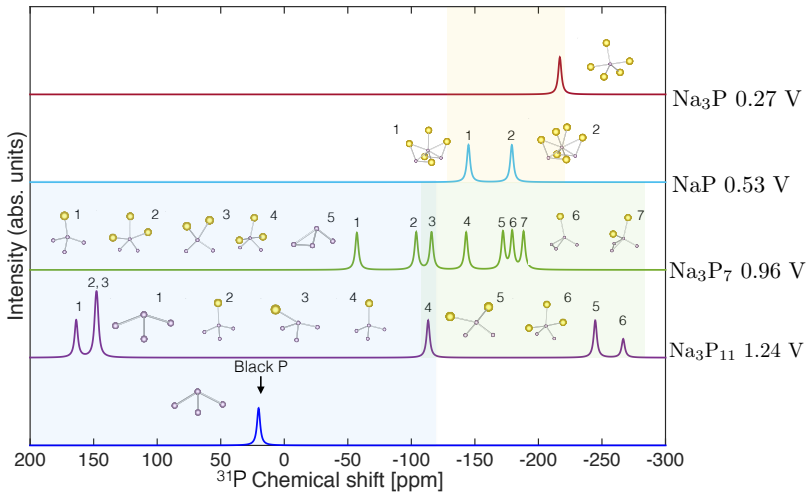

Figure 11: Calculated ^{31}P NMR chemical shifts, referenced using $\sigma_{ref.}$ obtained from Figure 5, for various Na-P compounds showing the change in chemical shift as the local environment of phosphorus changes. For visualisation purposes a Lorentzian broadening is assigned to the calculated ^{31}P NMR parameters. For each crystallographic site a cluster with a radius of 3 Å is shown and labeled accordingly. The background has been coloured as in Figure 6 to emphasise regions in the chemical shift associated with specific atomic arrangements. Despite the similarities to the Li-P, it may be more difficult to experimentally differentiate the mid and high sodiated regions due to a more similar chemical shift.

Aluminium doping of phosphorus

In order to suggest a way for improving the electrical conductivity of phosphorus anodes we have tested the effect of different extrinsic dopants on the electronic DOS of Li-P compounds by performing interstitial defects AIRSS searches. The initial generated structures were composed of the underlying perfect crystal plus the interstitial element positioned randomly. Consequently, the ionic positions were relaxed keeping the lattice vectors fixed. The electronic DOS of the lowest-energy structures were then calculated using OptaDOS.

Silicon and aluminium interstitial defect searches were carried out in a $2 \times 2 \times 1$ LiP supercell composed of 32 LiP formula units, we denote these structures as 32LiP + 1Si and 32LiP + 1Al, respectively. The eDOS calculation revealed that the aluminium point defect introduces electronic states at the Fermi energy (E_F), whereas the silicon defect introduces states within the band gap but with the eDOS remaining zero at E_F. To further investigate the effect of Al doping, AIRSS searches were performed in larger Li-P cells with different Li concentrations. The cells were chosen to be large enough to allow a maximum stress of ca. 0.5 GPa. Figure 12 shows the resulting eDOS of 8LiP_7 + 1Al, 64LiP + 1Al and 36Li_3P + 1Al for the lowest-energy structure resulting from the searches. AIRSS found the Al preferred site in LiP_7 between the phosphorus tubes and coordinated to 4 P atoms. In the case of Li_1P_1, the aluminium ion is found between the helical P chains. The environment of the Al atom in the Li_3P structure is more difficult to define. To clarify, we report the coordination number of the aluminium ion for all the structures in Table 5. The CIF files of the aluminium doped structures obtained by AIRSS can be found in the Supporting Information.

Table 5: Coordination number (CN) of the the aluminium ion for all the Li-P doped phases. A cut-off of 3 Å has been used.

Structure	P CN	Li CN
8LiP_7 + 1Al	4	–
64LiP + 1Al	4	4
36Li_3P + 1Al	3	8

From Figure 12, we learn that the formed Li-P compounds with different Li concentrations exhibit finite electronic DOS at E_F, suggesting that doping phosphorus with aluminium could

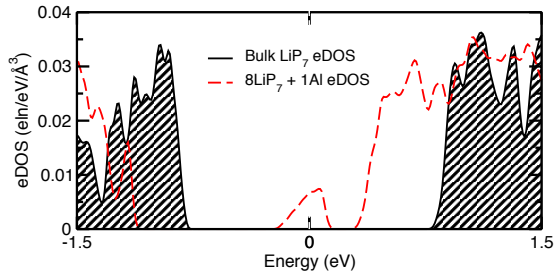

(a) 8LiP$_7$ + 1Al eDOS

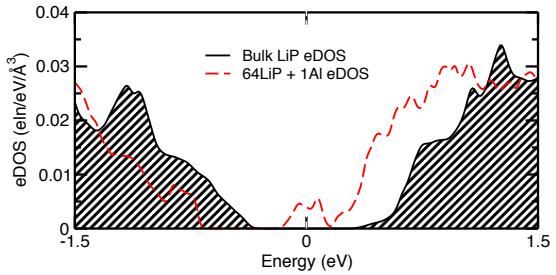

(b) 64LiP + 1Al eDOS

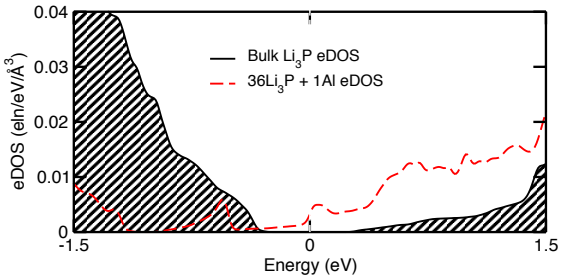

(c) 36Li$_3$P + 1Al eDOS

Figure 12: Electronic density of states in the vicinity of E_F for different Li-P compounds found on the convex hull (black line - dashed background) and Li-P with one aluminium interstitial defect (dashed red line). A finite electronic DOS is found at the Fermi energy for the Li-P compounds + Al, contrary to pristine Li-P compounds which exhibit band gaps around the Fermi level.

increase the electronic conductivity of the anode, thus improving its performance.

Discussion

We have presented a study of Li-P and Na-P systems using AIRSS and atomic species swapping of ICSD structures. We have shown that the combination of the two methods allows us to have access not only to the ground state structures, but also to metastable phases found close to the convex hull. These structures might form at room temperature and non-equilibrium conditions, *e.g.*, during lithiation/sodiation. The aim of this work is to elucidate the structural evolution of phosphorus anodes during the lithiation/sodiation as well as to give insights into their electronic structure, some of these aspects are discussed below.

The method of AIRSS + atomic species swapping has been shown to predict a variety of locally stable phases in the Li-P system (see Table 1 for full description). Combining the known phases with those predicted in this work, we are enabled to catalogue phosphorus ionic arrangements according to their lithium concentration. This has proved to be extremely valuable when attempting to understand electrochemical processes, as has been recently shown in Ref. 31 for LiS batteries. Our findings suggest that the lithiation mechanism proposed in Ref. 20, Black P $\rightarrow$ $Li_xP$$\rightarrow$LiP$\rightarrow$$Li_2P$$\rightarrow$$Li_3P$, could be reinterpreted in terms of tubes, cages and 3-D networks $\rightarrow$ chains and broken chains $\rightarrow$ P dumbbells $\rightarrow$ isolated P ions. Moreover, phases found by our structure searching can clarify possible intermediate structures in a more robust way. Park *et al.*[20] predicted the existence of a metastable Li_2P structure based on the appearance of a XRD peak at $2\theta \approx 22.5^\circ$ which corresponded to a molar ratio of Li:P 2 at 0.63 V. Our Li_2P–$P2_1/c$ structure exhibits a high intensity predominant peak at $2\theta \approx 25^\circ$, a discrepancy which can be attributed to the difference between the DFT and experimental lattice parameters.

The convex hull of the Na-P system predicts a locally stable NaP_5–Pnma phase which is very close to the convex hull; this phase has been synthesised at high-pressure.[66] A new phase, Na_5P_4, with C2/m symmetry is predicted to be stable by the convex hull construction. The phonon disper-

sion of the stable phase, Na_5P_4–C2/m, and the Li_4P_3–$P2_12_12_1$ metastable phase found very close to the convex hull suggest that these predicted structures are mechanically stable and might be observed in future experiments.

Red phosphorus is an experimentally interesting and low-cost alternative to black P for LIBs and NIBs. The convex hull is barely affected by the change of allotrope (i.e., by changing the P chemical potential). The insertion voltage however, was lowered from 1.5 to 1.2 V in the case of Li-P. The lattice parameters of red P are overestimated due to the absence of dispersion forces. The addition of SEDCs to all the compounds affects the calculation of the energetics of the system. Furthermore, we also found that the convex hull did not change when using the red P chemical potential with fixed experimental lattice parameters

NMR chemical shielding calculations reveal a general trend in the local environment change of both Li-P and Na-P systems as lithium/sodium content is increased. For Li-P the chemical shift range was roughly divided in three regions, where each region was correlated to distinct local ionic arrangements. These calculations were driven by the experimental ability of measuring NMR shifts, where the assignment of the local environments of the probed ion can be particularly challenging. Na-P shows a similar trend, as can be appreciated in Figure 11, but due to overlap between the regions mainly due to the wide range of Na_3P_{11} peaks, it may be more difficult to assign experimental data. We have considered the effect of aluminium doping to the limiting case of Na_3P. Our findings show that the effect of Al to Na_3P is not as obvious as in Li_3P. Although we see finite electronic states at E_F, these are part of a dip in the DOS at the vicinity of E_F, suggesting that these could arise due to the inability of PBE–DFT to correctly reproduce the band gap.

Li-P and Na-P exhibit relatively high average voltage profiles, which in principle leads to a lower voltage of the full cell and a reduced energy density. The Na-P voltage profile differs from the Li-P profile, the voltage drops to 0.28 V in the case of the Na_3P phase, whereas in the case of Li-P it drops to 0.8 V at the same lithium concentration. Despite this disadvantage, high voltages prevent the formation of Li dendrites, thus enhancing the safety of the battery. A second advantage of high voltages versus lithium metal, is the prevention of electrochemical reduction of the

electrolyte as SEI forms, which can improve the cyclability of the battery.[3] Another important aspect to consider is the volume change of P under lithiation/sodiation which may affect the stability of the SEI. The fully lithiated/sodiated Li_3P and Na_3P phases expand approximately 200% and 390% respectively. In the case of Li, this is considerably less than other Li intermetallics such as silicon where the volume expansion can reach more than 300%. However, the volume expansion of Na_3P is comparable to the one achieved by $Na_{15}Sn_4$, where the volume expansion is 420% but accommodating 3.5 sodium ions per Sn.

Despite several advantages, pure phosphorus shows a relatively poor cyclability.[20,21] Park *et al.*[20] attributed the low performance of phosphorus anodes to its low electronic conductivity. Sun *et al.*[21] showed that black P samples exhibit good conductivity properties, and put the low performance of the anode down to the non-crystallinity of the samples. Our results show that even for low concentrations of Li, Li-P compounds can exhibit a relatively large band gap, *e.g.*, 1.7 eV for LiP_7, compared to the experimental 0.33 eV of black P, hinting than the conducting properties of black P can be worsened as the anode is lithiated. In order to address this, we have sought to reduce the band gap of Li-P compounds by doping them with aluminium. Furthermore, we have performed a preliminary study on the effect of Ge and Ga doping on Li-P compounds electronic structure, where results show a similar behaviour as Si and Al respectively. 32LiP +1Ga exhibits a larger eDOS at E_F compared to 32LiP +1Al, 22.88 eln/cell and 10.78 eln/cell respectively. However, the lighter weight and high abundance of aluminium make it a promising dopant.

Summary

We have presented above an *ab initio* study of phosphorus anodes for Li and Na-ion batteries and proposed a theoretical lithiation/sodiation process using the structure prediction AIRSS method. Our searches reveal the existence of a variety of metastable structures which can appear in out-of-equilibrium processes such as charge and discharge. In particular, a Li_4P_3–$P2_12_12_1$ AIRSS structure found to lie very close to the convex hull and a new Na_5P_4–C2/m structure obtained by

the species swapping method found stable at 0 K. The dynamical stability of these structures was probed by phonon calculations. Our calculations showed a high theoretical voltage vs Li metal for Li-P, which makes phosphorus a good candidate for safe anodes at high rate charges. We have calculated ^{31}P NMR chemical shielding and related them to local structure arrangements, which combined with future ^{31}P NMR experiments can elucidate lithiation and sodiation mechanisms. Finally we have studied the effect of dopants on the electronic structure of Li-P compounds, where we conclude that doping the anode with aluminium can improve its electrochemical behaviour.

Acknowledgement

M.M. and A.J.M. acknowledge the support from the Winton Programme for the Physics of Sustainability. K.J.G thanks the Winston Churchill Foundation of the United States and the Herchel Smith Foundation. C.J.P. was funded by the Engineering and Physical Sciences Research Council (EPSRC) of the UK, grant number EP/G007489/2. C.J.P. is also supported by the Royal Society through a Royal Society Wolfson Research Merit award.

Supporting Information Available

Additional research data supporting this publication, including CIF files of the structures obtained by AIRSS and species-swapping methods, are available as supplementary files at the journal's website. This material is available free of charge via the Internet at `http://pubs.acs.org/`.

References

(1) Chu, S.; Majumdar, A. Opportunities and Challenges for a Sustainable Energy Future. *Nature* **2012**, *488*, 294–303.

(2) Scrosati, B.; Abraham, K.; van Schalkwijk, W.; Hassoun, J. *Lithium Batteries: Advanced Technologies and Applications*; The ECS Series of Texts and Monographs; Wiley, 2013.

(3) Nitta, N.; Yushin, G. High-Capacity Anode Materials for Lithium-Ion Batteries: Choice of Elements and Structures for Active Particles. *Part. Part. Syst. Char.* **2014**, *31*, 317–336.

(4) Kim, Y.; Kim, D.; Kang, S. Experimental and First-Principles Thermodynamic Study of the Formation and Effects of Vacancies in Layered Lithium Nickel Cobalt Oxides. *Chem. Mater.* **2011**, *23*, 5388–5397.

(5) McDowell, M. T.; Lee, S. W.; Nix, W. D.; Cui, Y. 25th Anniversary Article: Understanding the Lithiation of Silicon and Other Alloying Anodes for Lithium-Ion Batteries. *Adv. Mater.* **2013**, *25*, 4966–4985.

(6) Kasavajjula, U.; Wang, C.; Appleby, A. J. Nano- and Bulk-Silicon-Based Insertion Anodes for Lithium-Ion Secondary Cells. *J. Power Sources* **2007**, *163*, 1003 – 1039.

(7) Zhang, W.-J. A Review of the Electrochemical Performance of Alloy Anodes for Lithium-ion Batteries. *J. Power Sources* **2011**, *196*, 13 – 24.

(8) Szczech, J. R.; Jin, S. Nanostructured Silicon for High Capacity Lithium Battery Anodes. *Energy Environ. Sci.* **2011**, *4*, 56–72.

(9) Qian, J.; Qiao, D.; Ai, X.; Cao, Y.; Yang, H. Reversible 3-Li Storage Reactions of Amorphous Phosphorus as High Capacity and Cycling-stable Anodes for Li-ion Batteries. *Chem. Commun.* **2012**, *48*, 8931–8933.

(10) Obrovac, M. N.; Christensen, L. Structural Changes in Silicon Anodes during Lithium Insertion/Extraction. *Electrochem. Solid-State Lett.* **2004**, *7*, A93–A96.

(11) Klein, F.; Jache, B.; Bhide, A.; Adelhelm, P. Conversion Reactions for Sodium-Ion Batteries. *Phys. Chem. Chem. Phys.* **2013**, *15*, 15876–15887.

(12) Hong, S. Y.; Kim, Y.; Park, Y.; Choi, A.; Choi, N.-S.; Lee, K. T. Charge Carriers in Rechargeable Batteries: Na Ions vs. Li Ions. *Energy Environ. Sci.* **2013**, *6*, 2067–2081.

(13) Stevens, D. A.; Dahn, J. R. The Mechanisms of Lithium and Sodium Insertion in Carbon Materials. *J. Electrochem. Soc.* **2001**, *148*, A803–A811.

(14) Brauer, G.; Zintl, E. Metals and Alloys. 23. Constitution of Phosphides, Arsenides, Antimonides and Bismuthides of Li, Na and K. *Z. Phys. Chem. (Leipzig) Abt. B* **1937**, *37(5/6)*, 307–1314.

(15) Dong, Y.; Di Salvo, F. J. Reinvestigation of Na_3P Based on Single-Crystal Data. *Acta Crystallogr. Sect. E: Struct. Rep. Online* **2005**, *61*, i223–i224.

(16) Li, L.; Yu, Y.; Ye, G. J.; Ge, Q.; Ou, X.; Wu, H.; Feng, D.; Chen, X. H.; Zhang, Y. Black Phosphorus Field-Effect Transistors. *Nat. Nanotechnol.* **2014**, *9*, 372–377.

(17) Kulish, V. V.; Malyi, O. I.; Persson, C.; Wu, P. Phosphorene as an Anode Material for Na-Ion Batteries: A First-Principles Study. *Phys. Chem. Chem. Phys.* **2015**, *17*, 13921–13928.

(18) Zhao, S.; Kang, W.; Xue, J. The Potential Application of Phosphorene as an Anode Material in Li-Ion Batteries. *J. Mater. Chem. A* **2014**, *2*, 19046–19052.

(19) Sun, J.; Lee, H.-W.; Pasta, M.; Yuan, H.; Zheng, G.; Sun, Y.; Li, Y.; Cui, Y. A Phosphorene–Graphene Hybrid Material as a High-Capacity Anode for Sodium-Ion Batteries. *Nat. Nanotechnol.* **2015**,

(20) Park, C.-M.; Sohn, H.-J. Black Phosphorus and its Composite for Lithium Rechargeable Batteries. *Adv. Mater.* **2007**, *19*, 2465–2468.

(21) Sun, L.-Q.; Li, M.-J.; Sun, K.; Yu, S.-H.; Wang, R.-S.; Xie, H.-M. Electrochemical Activity of Black Phosphorus as an Anode Material for Lithium-Ion Batteries. *J. Phys. Chem. C* **2012**, *116*, 14772–14779.

(22) Marino, C.; Debenedetti, A.; Fraisse, B.; Favier, F.; Monconduit, L. Activated-phosphorus as new electrode material for Li-ion batteries. *Electrochem. Commun.* **2011**, *13*, 346 – 349.

(23) Marino, C.; Boulet, L.; Gaveau, P.; Fraisse, B.; Monconduit, L. Nanoconfined Phosphorus in Mesoporous Carbon as an Electrode for Li-Ion Batteries: Performance and Mechanism. *J. Mater. Chem.* **2012**, *22*, 22713–22720.

(24) Qian, J.; Wu, X.; Cao, Y.; Ai, X.; Yang, H. High Capacity and Rate Capability of Amorphous Phosphorus for Sodium Ion Batteries. *Angew. Chem. Int. Ed.* **2013**, *52*, 4633–4636.

(25) Ramireddy, T.; Xing, T.; Rahman, M. M.; Chen, Y.; Dutercq, Q.; Gunzelmann, D.; Glushenkov, A. M. Phosphorus–Carbon Nanocomposite Anodes for Lithium-Ion and Sodium-Ion Batteries. *J. Mater. Chem. A* **2015**, *3*, 5572–5584.

(26) Yu, Z.; Song, J.; Gordin, M. L.; Yi, R.; Tang, D.; Wang, D. Phosphorus-Graphene Nanosheet Hybrids as Lithium-Ion Anode with Exceptional High-Temperature Cycling Stability. *Advanced Science* **2015**, *2*, n/a–n/a.

(27) Song, J.; Yu, Z.; Gordin, M. L.; Hu, S.; Yi, R.; Tang, D.; Walter, T.; Regula, M.; Choi, D.; Li, X.; Manivannan, A.; Wang, D. Chemically Bonded Phosphorus/Graphene Hybrid as a High Performance Anode for Sodium-Ion Batteries. *Nano Letters* **2014**, *14*, 6329–6335, PMID: 25354313.

(28) Jung, S. C.; Han, Y.-K. Thermodynamic and Kinetic Origins of Lithiation-Induced Amorphous-to-Crystalline Phase Transition of Phosphorus. *J. Phys. Chem. C* **2015**, *119*, 12130–12137.

(29) Hembram, K.; Jung, H.; Yeo, B. C.; Pai, S. J.; Kim, S.; Lee, K.-R.; Han, S. S. Unraveling the Atomistic Sodiation Mechanism of Black Phosphorus for Sodium Ion Batteries by First-Principles Calculations. *J. Phys. Chem. C* **2015**, *119*, 15041–15046.

(30) Ogata, K.; Salager, E.; Kerr, C. J.; Fraser, A. E.; Ducati, C.; Morris, A. J.; Hofmann, S.; Grey, C. P. Revealing Lithium–Silicide Phase Transformations in Nano-Structured Silicon-Based Lithium Ion Batteries via in Situ NMR Spectroscopy. *Nat Commun* **2014**, *5*.

(31) See, K. A.; Leskes, M.; Griffin, J. M.; Britto, S.; Matthews, P. D.; Emly, A.; Van der Ven, A.; Wright, D. S.; Morris, A. J.; Grey, C. P.; Seshadri, R. Ab Initio Structure Search and in Situ 7Li NMR Studies of Discharge Products in the Li-S Battery System. *J. Am. Chem. Soc.* **2014**, *136*, 16368–16377, PMID: 25384082.

(32) Jung, H.; Allan, P. K.; Hu, Y.-Y.; Borkiewicz, O. J.; Wang, X.-L.; Han, W.-Q.; Du, L.-S.; Pickard, C. J.; Chupas, P. J.; Chapman, K. W.; Morris, A. J.; Grey, C. P. Elucidation of the Local and Long-Range Structural Changes that Occur in Germanium Anodes in Lithium-Ion Batteries. *Chem. Mater.* **2015**, *27*, 1031–1041.

(33) Pourpoint, F.; Kolassiba, A.; Gervais, C.; Azaïs, T.; Bonhomme-Coury, L.; Bonhomme, C.; Mauri, F. First Principles Calculations of NMR Parameters in Biocompatible Materials Science: The Case Study of Calcium Phosphates, β-and γ-Ca (PO3) 2. Combination with MAS-J Experiments. *Chem. Mater.* **2007**, *19*, 6367–6369.

(34) Sneddon, S.; Dawson, D. M.; Pickard, C. J.; Ashbrook, S. E. Calculating NMR Parameters in Aluminophosphates: Evaluation of Dispersion correction schemes. *Phys. Chem. Chem. Phys.* **2014**, *16*, 2660–2673.

(35) Pickard, C. J.; Needs, R. J. High-Pressure Phases of Silane. *Phys. Rev. Lett.* **2006**, *97*, 045504.

(36) Pickard, C. J.; Needs, R. J. *Ab Initio* Random Structure Searching. *J. Phys.: Condens. Matter* **2011**, *23*, 053201.

(37) Morris, A. J.; Grey, C. P.; Pickard, C. J. Thermodynamically Stable Lithium Silicides and Germanides From Density Functional Theory Calculations. *Phys. Rev. B* **2014**, *90*, 054111.

(38) Morris, A. J.; Pickard, C. J.; Needs, R. J. Hydrogen/silicon Complexes in Silicon From Computational Searches. *Phys. Rev. B* **2008**, *78*, 184102.

(39) Morris, A. J.; Needs, R. J.; Salager, E.; Grey, C. P.; Pickard, C. J. Lithiation of Silicon via Lithium Zintl-Defect Complexes From First Principles. *Phys. Rev. B* **2013**, *87*, 174108.

(40) Clark, S. J.; Segall, M. D.; Pickard, C. J.; Hasnip, P. J.; Probert, M. J.; Refson, K.; Payne, M. First Principles Methods Using CASTEP. *Z. Kristall.* **2005**, *220*, 567–570.

(41) Perdew, J. P.; Burke, K.; Ernzerhof, M. Generalized Gradient Approximation Made Simple. *Phys. Rev. Lett.* **1996**, *77*, 3865–3868.

(42) Monkhorst, H. J.; Pack, J. D. Special Points for Brillouin-Zone Integrations. *Phys. Rev. B* **1976**, *13*, 5188–5192.

(43) Aydinol, M. K.; Kohan, A. F.; Ceder, G.; Cho, K.; Joannopoulos, J. *Ab Initio* Study of Lithium Intercalation in Metal Oxides and Metal Dichalcogenides. *Phys. Rev. B* **1997**, *56*, 1354–1365.

(44) Pickard, C.; Mauri, F. All-Electron Magnetic Response With Pseudopotentials: NMR Chemical Shifts. *Phys. Rev. B* **2001**, *63*, 245101.

(45) Morris, A. J.; Nicholls, R. J.; Pickard, C. J.; Yates, J. R. OptaDOS: A Tool for Obtaining Density of States, Core-Level and Optical Spectra From Electronic Structure Codes. *Comput. Phys. Commun.* **2014**, *185*, 1477 – 1485.

(46) Pickard, C. J.; Payne, M. C. Extrapolative Approaches to Brillouin-Zone Integration. *Phys. Rev. B* **1999**, *59*, 4685–4693.

(47) Pickard, C. J.; Payne, M. C. Second-Order $\mathbf{k} \cdot \mathbf{p}$ Perturbation Theory With Vanderbilt Pseudopotentials and Plane Waves. *Phys. Rev. B* **2000**, *62*, 4383–4388.

(48) Refson, K.; Tulip, P. R.; Clark, S. J. Variational Density-Functional Perturbation Theory for Dielectrics and Lattice Dynamics. *Phys. Rev. B* **2006**, *73*, 155114.

(49) McNellis, E. R.; Meyer, J.; Reuter, K. Azobenzene at Coinage Metal Surfaces: Role of Dispersive Van Der Waals Interactions. *Phys. Rev. B* **2009**, *80*, 205414.

(50) Grimme, S. Semiempirical GGA-Type Density Functional Constructed With a Long-Range Dispersion Correction. *J. Comput. Chem.* **2006**, *27*, 1787–1799.

(51) Appalakondaiah, S.; Vaitheeswaran, G.; Lebègue, S.; Christensen, N. E.; Svane, A. Effect of Van der Waals Interactions on the Structural and Elastic Properties of Black Phosphorus. *Phys. Rev. B* **2012**, *86*, 035105.

(52) Reckien, W.; Janetzko, F.; Peintinger, M. F.; Bredow, T. Implementation of Empirical Dispersion Corrections to Density Functional Theory for Periodic Systems. *J. Comput. Chem.* **2012**, *33*, 2023–2031.

(53) Bučko, T.; Lebègue, S.; Hafner, J.; Ángyán, J. G. Tkatchenko-Scheffler van der Waals Correction Method with and without Self-Consistent Screening Applied to Solids. *Phys. Rev. B* **2013**, *87*, 064110.

(54) Von Schnering, H.; Wichelhaus, W. Die Lithiumphosphide LiP 5 und LiP 7. Zur Chemie und Strukturchemie der Phosphide und Polyphosphide, 4. *Naturwissenschaften* **1972**, *59*, 78–79.

(55) Honle, W.; Manriquez, V.; Meyer, T.; von Schnering, H. Crystalline and Plastic-Crystalline Phases of Alkali Metal Phosphides M_3P_7. *Z. Kristallogr.* **1983**, *164*, 104–106.

(56) Honle, W.; von Schnering, H. Chemistry and Structural Chemistry of Phosphides and Polyphosphides. 23. Structure of LiP and KSb. *Z. Kristallogr.* **1981**, *155*, 307–1314.

(57) Dong, Y.; DiSalvo, F. J. Reinvestigation of Trilithium Phosphide, Li_3P. *Acta Crystallographica Section E* **2007**, *63*, i97–i98.

(58) Wichelhaus, W.; von Schnering, H. Na_3P_{11}, ein Phosphid mit isolierten P_{11}^{-3}–Gruppen. *Naturwissenschaften* **1973**, *60*, 104–104.

(59) Ozisik, H.; Colakoglu, K.; Deligoz, E.; Ozisik, H. First Principles Study on the Structural, Electronic, and Elastic Properties of Na–As Systems. *Solid State Commun.* **2011**, *151*, 1349 – 1354.

(60) Ivanov, A. S.; Morris, A. J.; Bozhenko, K. V.; Pickard, C. J.; Boldyrev, A. I. Inorganic

Double-Helix Structures of Unusually Simple Lithium–Phosphorus Species. *Angew. Chem. Int. Ed.* **2012**, *51*, 8330–8333.

(61) auf der Günne, J. S.; Kaczmarek, S.; van Wüllen, L.; Eckert, H.; Paschke, D.; Foecker, A. J.; Jeitschko, W. Solid-State NMR Connectivity Studies in Dipolarly Coupled Inorganic Networks: Crystal Structure and Site Assignments for the Lithium Polyphosphide LiP5. *J. Solid State Chem.* **1999**, *147*, 341 – 349.

(62) Laskowski, R.; Blaha, P.; Tran, F. Assessment of DFT Functionals With NMR Chemical Shifts. *Phys. Rev. B* **2013**, *87*, 195130.

(63) Rehr, A.; Guerra, F.; Parkin, S.; Hope, H.; Kauzlarich, S. M. KSb2, a New Structure Composed of Ribbons of Edge-Shared Six-Membered Sb Rings. *Inorg. Chem.* **1995**, *34*, 6218–6220.

(64) Abicht, H.-P.; H nle, W.; v. Schnering, H. G. Zur Chemie und Strukturchemie von Phosphiden und Polyphosphiden. 36. Tetrakaliumhexaphosphid: Darstellung, Struktur und Eigenschaften von α-K4P6 und β-K4P6. *Z. Anorg. Allg. Chem.* **1984**, *519*, 7–23.

(65) von Schnering, H. G.; Hartweg, M.; Hartweg, U.; Honle, W. K4P3, eine Verbindung mit dem Radikalanion. *Angew. Chem – Ger. Edit.* **1989**, *101*, 98–99.

(66) Chen, X.; Yamanaka, S. High-Pressure Synthesis and Crystal Structures of Two New Polyphosphides, NaP_5 and CeP_5. *J. Alloys Compd.* **2004**, *370*, 110 – 113.

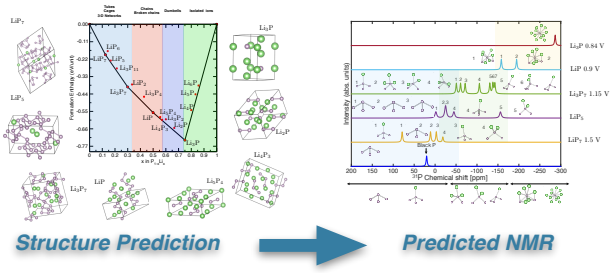

Figure 13: ToC